LABORATORY INVESTIGATION

Transarterial Embolization of Liver Cancer in a Transgenic Pig Model

Fuad Nurili, MD, Sebastien Monette, DVM, MVSc, Adam O. Michel, MVSc, DVM, DrMedVet, Achiude Bendet, MD, Olca Basturk, MD, Gokce Askan, MD, Christopher Cheleuitte-Nieves, PhD, DVM, Hooman Yarmohammadi, MD, Aaron W.P. Maxwell, MD, Etay Ziv, MD, PhD, Kyle M. Schachtschneider, PhD, Ron C. Gaba, MD, MS, Lawrence B. Schook, PhD, Stephen B. Solomon, MD, and F. Edward Boas, MD, PhD

ABSTRACT

Purpose: To develop and characterize a porcine model of liver cancer that could be used to test new locoregional therapies.

Materials and Methods: Liver tumors were induced in 18 Oncopigs (transgenic pigs with Cre-inducible $TP53^{R167H}$ and $KRAS^{G12D}$ mutations) by using an adenoviral vector encoding the Cre-recombinase gene. The resulting 60 tumors were characterized on multiphase contrast-enhanced CT, angiography, perfusion, micro-CT, and necropsy. Transarterial embolization was performed using 40–120 μm (4 pigs) or 100–300 μm (4 pigs) Embosphere microspheres. Response to embolization was evaluated on imaging. Complications were determined based on daily clinical evaluation, laboratory results, imaging, and necropsy.

Results: Liver tumors developed at 60/70 (86%) inoculated sites. Mean tumor size was 2.1 cm (range, 0.3–4 cm) at 1 week. Microscopically, all animals developed poorly differentiated to undifferentiated carcinomas accompanied by a major inflammatory component, which resembled undifferentiated carcinomas of the human pancreatobiliary tract. Cytokeratin and vimentin expression confirmed epithelioid and mesenchymal differentiation, respectively. Lymph node, lung, and peritoneal metastases were seen in some cases. On multiphase CT, all tumors had a hypovascular center, and 17/60 (28%) had a hypervascular rim. After transarterial embolization, noncontrast CT showed retained contrast medium in the tumors. Follow-up contrast-enhanced scan showed reduced size of tumors after embolization using either 40–120 μm or 100–300 μm Embosphere microspheres, while untreated tumors showed continued growth.

Conclusions: Liver tumors can be induced in a transgenic pig and can be successfully treated using bland embolization.

From the Interventional Radiology Service (F.N., A.B., H.Y., A.W.P.M., E.Z., S. B.S, F.E.B.), Department of Radiology, Memorial Sloan Kettering Cancer Center, 1275 York Avenue, New York, NY 10065; Laboratory of Comparative Pathology (S.M., A.O.M.), Memorial Sloan Kettering Cancer Center, The Rockefeller University, Weill Cornell Medicine, New York, New York; Department of Pathology (O.B., G.A.), Memorial Sloan Kettering Cancer Center, 1275 York Avenue, New York, NY 10065; Center of Comparative Medicine and Pathology (C.C.-N.), Sloan Kettering Institute, New York, New York; Department of Radiology (K.M.S., R.C.G.), University of Illinois at Chicago, Chicago, Illinois; and Department of Animal Sciences (L.B.S.), University of Illinois at Urbana–Champaign, Urbana, Illinois. Received June 10, 2020; final revision received and accepted September 10, 2020. **Address correspondence to** F. E.B.; E-mail: boasf@mskcc.org

H.Y. is an advisory board member of Becton, Dickinson and Company (Franklin Lakes, New Jersey). R.C.G. receives research support from Guerbet LLC (Princeton, New Jersey) and Janssen Research & Development LLC (Raritan, New Jersey). L.B.S. receives personal fees from Sus Clinicals, Inc (Cincinnati, Ohio). S.B.S. is a paid consultant for Johnson & Johnson (New Brunswick, New Jersey), Aperture Medical LLC (Sandy, Utah), XACT Robotics Ltd. (Caesarea, Israel), Innoblative Designs, Inc (Chicago, Illinois), EndoWays (Or Yehuda, Israel), and Varian Medical Systems (Palo Alto, California); receives grants from GE Healthcare (Chicago, Illinois), AngioDynamics (Latham, New York), ELESTA GmbH (Bad Ragaz, Switzerland), and Johnson & Johnson; and is a shareholder in Aspire Bariatrics (King of Prussia), Aperture Medical LLC, Johnson & Johnson, Immunomedics, Inc (Morris Plains, New Jersey), Impulse Medical Technologies, Inc (Buckley, Washington), Motus GI (Fort Lauderdale, Florida), and Progenics Pharmaceuticals, Inc (Tarrytown, New York). F.E.B. is a co-founder of Claripacs, LLC (New York, New York); receives research support from GE Healthcare, Bayer (Leverkusen, Germany), Steba Biotech (Luxembourg), and Terumo Medical Corporation (Somerset, New Jersey); receives research grants and is a paid speaker for Society of Interventional Oncology; is an investor in Labdoor, Inc (San Francisco, California), Qventus, Inc (Mountain View, California), CloudMedx (Palo Alto, California), Notable Labs (Foster City, California), and Xgenomes (Cambridge, Massachusetts); is the inventor and assignee on US patent 8233586; and is an inventor on US provisional patent applications 62/754,139 and 62/817,116. None of the other authors have identified a conflict of interest.

Abstract from the SIR 2020 Annual Scientific Meeting published in *JVIR* 2020; 31:S90–S91.

Figures E1–E4 and Tables E1 and E2 can be found by accessing the online version of this article on *www.jvir.org* and clicking on the Supplemental Material tab.

J Vasc Interv Radiol 2021; ■:1–8

https://doi.org/10.1016/j.jvir.2020.09.011

ABBREVIATION

HCC = hepatocellular carcinoma

Current intra-arterial therapies for liver cancer or liver metastases—embolization, chemoembolization, and radioembolization—have several limitations, including a high rate of recurrence, damage to normal liver, and inability to treat extrahepatic disease. A wide range of new therapies have been proposed to address these limitations, including new embolic agents (1,2), devices for local drug delivery (3–5), intra-arterial drugs (6–10), intra-arterial virus (11), and intravascular ablation modalities (12–15).

Realistic animal models are critical to develop and optimize innovative locoregional therapies for liver cancer. Existing animal models do not always accurately reflect outcomes in humans. Hepatocellular carcinoma (HCC) can be induced in rats and mice (16,17). However, lobar embolization in rats (17) results in liver and lung necrosis and a mortality rate of 56%. New cancer therapies developed in rodents have a high failure rate when translated to humans (18). The rabbit VX2 model is currently the most commonly used model for testing intra-arterial therapies in the liver. However, rabbits generally have different physiology (19,20) and usually require higher weight-based drug dosing (21,22) than humans.

This article presents a new pig model of liver cancer using the Oncopig (23,24), a transgenic pig with Cre-recombinase–inducible $TP53^{R167H}$ and $KRAS^{G12D}$ mutations. In contrast to rodents and rabbits, pigs have similar size, physiology (19,20), drug dosing (21,22), and immune response (25,26) to humans. Locoregional therapy in pigs can be performed using the same size catheters and devices that are used in humans. This porcine model could enable rapid testing and iteration of new devices, drugs, and techniques that are not yet ready for human trials.

MATERIALS AND METHODS

Animals

The Institutional Animal Care and Use Committee approved all research procedures. The animal facility has AAALAC accreditation and operates in compliance with the Guide for the Care and Use of Laboratory Animals (27). Eighteen female Oncopigs (transgenic pigs with Cre-inducible $TP53^{R167H}$ and $KRAS^{G12D}$ mutations) were obtained from the University of Illinois or the National Swine Resource and Research Center at the University of Missouri. All procedures and imaging were performed under general anesthesia with perioperative analgesia. Tumor induction was performed when the pigs were 8–22 weeks old. The overall study design is shown in **Figure E1** (available online on the article's Supplemental Material page at *www.jvir.org*).

Tumor Induction (In Situ Method)

An 18-gauge core biopsy specimen of the liver was obtained under computed tomography (CT) or ultrasound guidance (1- or 2-cm core length; Temno Evolution; Merit Medical Systems, South Jordan, Utah) using coaxial technique (18 pigs). $TP53^{R167H}$ and $KRAS^{G12D}$ expression was induced by incubating the core biopsy specimen with an adenoviral vector carrying the Cre recombinase gene (10^9 pfu Ad5CMVCre-eGFP; University of Iowa Viral Vector Core, Iowa City, Iowa) for 20 minutes at room temperature in phosphate-buffered saline containing 15-mM calcium chloride (total fluid volume of 1 mL). Gelatin sponge (Surgifoam; Ethicon, Somerville, New Jersey) was then added using a 3-way stopcock, and the mixture (virus, core biopsy specimen, gelatin) was injected percutaneously back into the pig's liver through the biopsy needle, which was kept in place. At least 2 sites were inoculated in each liver. Inoculation sites were selected to be as far apart as possible, easy and safe to access, and deep enough to avoid leakage of injected material into the peritoneum.

Tumor Induction (Cell Line Method)

Autologous hepatocyte-derived cell lines were created in 8 pigs, as previously described (28,29). Briefly, liver resection was performed, and hepatocytes were purified. The hepatocytes were transformed using Ad5CMVCre-eGFP and then passaged in cell culture. Transformed cells (6×10^7) were mixed with gelatin sponge and injected percutaneously into the pig's liver under CT or ultrasound guidance. At least 2 sites were inoculated in each liver.

Multiphase Contrast-Enhanced CT

Five-phase contrast-enhanced CT was performed 1 and 2 weeks after tumor inoculation to monitor tumor growth and response to therapy (18 pigs; as described below, a subset of pigs was treated using transarterial embolization immediately after the 1-week scan). Noncontrast CT of the abdomen and pelvis was performed. Omnipaque 300 (2 mL/kg, maximum 150 mL; GE Healthcare, Chicago, Illinois) was power injected at 2–3 mL/s. The early arterial phase CT scan was obtained when the abdominal aorta reached 150 Hounsfield units. The late arterial phase was obtained 15 seconds after the early arterial phase. The portal venous phase was obtained 25 seconds after the late arterial phase scan. The delayed phase scan was obtained 90 seconds after the portal venous phase. All scans were obtained at 120 kVp.

Liver Tumor Perfusion

Hepatic artery and portal vein perfusion of the largest liver tumor in each pig (18 pigs) was estimated based on quantitative measurements from multiphase CT, as previously described (30).

Angiography, Cone-Beam CT, and Micro-CT

From femoral access, under fluoroscopic guidance, a 4-F catheter was advanced into the celiac artery, and an arteriogram was obtained. The 4-F catheter or a 2.4-F microcatheter was advanced into the hepatic artery, and an arteriogram was obtained. Cone-beam CT arteriography was performed during a breath hold after administering a paralytic agent (rocuronium 1–1.6 mg/kg intravenously). To obtain high-resolution micro-CT of tumor arteries, yellow silicone contrast medium (MICROFIL; Flow Tech, Inc, Carver, Massachusetts) was injected into the hepatic artery 2 weeks after tumor inoculation in a single pig with untreated liver tumors. The liver tumor was resected, and ex vivo micro-CT was performed at 85-μm resolution using a microCAT II micro-CT scanner (Imtek Corp, Oak Ridge, Tennessee).

Transarterial Embolization

One week after tumor inoculation, selective transarterial embolization of 1 liver tumor per pig was performed to stasis, using 40–120 μm (4 pigs) or 100–300 μm (4 pigs) Embosphere microspheres (Merit Medical Systems). Follow-up CT scan and necropsy were performed 1 week after embolization.

Safety Evaluation

Complications were determined based on daily clinical evaluation after treatment, CT scan, laboratory results (liver function tests, basic metabolic panel, complete blood count) before treatment and before necropsy, and necropsy.

Pathology

Two weeks after tumor inoculation, the final CT scan was obtained, the animals were euthanized, and the liver tumors were macroscopically examined, harvested, and fixed in 10% neutral buffered formalin (18 pigs). Complete necropsies were performed in 2 pigs. Following formalin fixation, sections of tumor were processed into paraffin blocks and sectioned at 5-μm thickness. Hematoxylin and eosin–stained sections were reviewed by both human (O.B., G.A.) and veterinary (A.O.M., S.M.) pathologists. Representative formalin-fixed paraffin-embedded tissue sections were immunolabeled with antibodies against cytokeratin AE1/AE3, vimentin, Iba1, arginase, and CD31 (**Table E1** [available online on the article's Supplemental Material page at *www.jvir.org*]).

Statistical Analysis

Tumor sizes were compared using 2-tailed t tests. Proportions were compared using Fisher exact test or χ^2 test. Statistical analysis was performed in Excel 2016 (Microsoft Corp, Redmond, Washington) and Mathematica 12 (Wolfram, Champaign, Illinois). P values $< .05$ were considered significant.

RESULTS

Imaging

Liver tumors developed at 60 of 70 sites (86%) that were inoculated. Mean tumor size was 2.1 cm (range, 0.3–4 cm) at 1 week. There was no significant difference in inoculation success rate ($P = .06$) or tumor size ($P = .47$) for sites inoculated using the in situ method (n = 48) or the cell line method (n = 22). There was a trend toward lower inoculation success rate with the cell line method (73%) compared with the in situ method (92%).

On multiphase contrast-enhanced CT, all tumors had a hypovascular center (**Fig 1a–e**), and 17 of 60 (28%) had a hypervascular rim (**Fig E2a** [available online on the article's Supplemental Material page at *www.jvir.org*]). Two tumors invaded the hepatic vein, and 1 tumor invaded the portal vein (**Fig E2b** [available online on the article's Supplemental Material page at *www.jvir.org*]).

Perfusion

Hepatic artery and portal vein perfusion to Oncopig liver tumors (**Fig E3** [available online on the article's Supplemental Material page at *www.jvir.org*]) overlaps with previously collected perfusion data on human HCC (30) and colorectal cancer liver metastases (31); 35% of human HCCs and 83% of human colorectal liver metastases fall within the range of hepatic artery and portal vein coefficients seen in Oncopig liver tumors.

Micro-CT

Micro-CT of untreated Oncopig liver tumors (**Fig 2**) shows that the tumors recruit blood supply from the hepatic artery and develop new tumor vascularity. The scan resolution is 85 μm, which is smaller than many embolic particles.

Pathology

Grossly, the tumors were solid, pale tan lesions involving the liver. Histopathology revealed poorly differentiated to undifferentiated carcinomas, accompanied by a major inflammatory component, in all 18 pigs (**Fig 3a–f**). Hematoxylin and eosin–stained sections (46 tumors) showed 4 different tumor morphologies: (*a*) numerous atypical epithelioid cells organized in hypercellular anastomosing islands (15 of 46 tumors); (*b*) small number of atypical epithelioid cells present as individual cells or very small clusters (21 of 46 tumors); (*c*) numerous spindle cells organized in hypercellular bundles with a smaller epithelioid

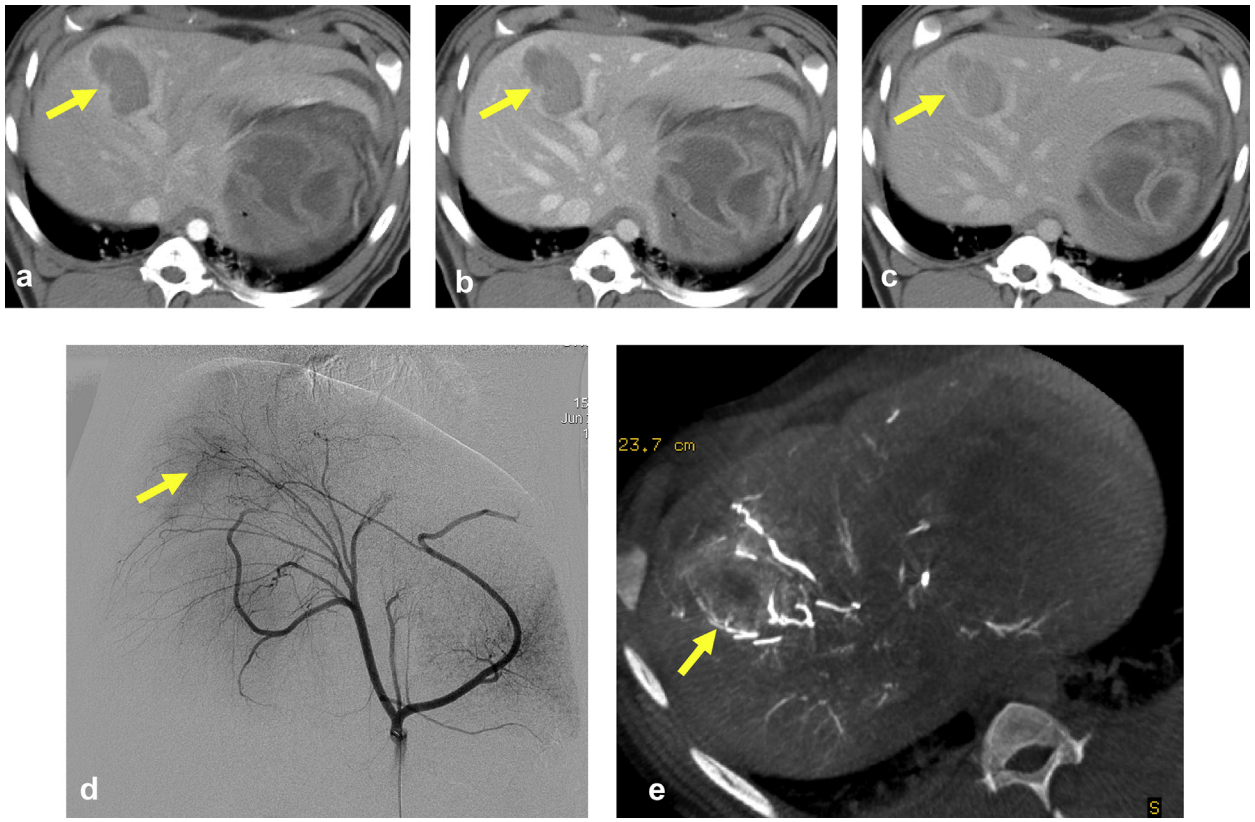

Figure 1. Imaging characteristics of an Oncopig liver tumor (arrows). Arterial **(a)**, portal venous **(b)**, and delayed phase **(c)** contrast-enhanced CT images as well as celiac angiography **(d)** and cone-beam CT **(e)** are shown. The tumor is hypovascular on CT, but mildly hypervascular on angiography and cone-beam CT.

cell component (7 of 46 tumors); (*d*) inflammation only, without atypical cells (3 of 46 tumors). There was no association between the tumor induction technique (in situ or cell line) and tumor morphology ($P = .44$).

All tumors had a strong inflammatory response that was composed of lymphocytic and plasmacytic inflammatory infiltrates, often surrounding neoplastic cells and infiltrating portal regions of the liver. In contrast, necrotic portions of the tumor were surrounded by histiocytes and neutrophils. Multinucleated giant cells were often noted in the tumors.

Immunohistochemistry revealed that neoplastic cells with an atypical epithelioid morphology had 2 distinct immunophenotypes. They were either cytokeratin AE1/AE3 and vimentin immunopositive (**Fig 3c, d**) or AE1/AE3 immunonegative and vimentin immunopositive. The spindle cells were AE1/AE3 immunonegative and vimentin immunopositive (**Fig E4** [available online on the article's Supplemental Material page at *www.jvir.org*]). Cytokeratin expression indicates epithelial differentiation, and vimentin expression indicates mesenchymal differentiation. Loss of cytokeratin expression, with maintenance of malignant cytologic features, suggests epithelial-to-mesenchymal transition. Tumor cells were immunonegative for Iba1, arginase, and CD31.

Metastases to lymph nodes, peritoneum, and lung were seen in some cases (**Fig 3e, f**). Two pigs had a complete necropsy, and an additional 3 pigs had incidentally noted extrahepatic tumors that were submitted to pathology. Histologically confirmed metastases were seen in the peritoneum (5 of 5 pigs), lymph nodes (2 of 5 pigs), lung (1 of 5 pigs), and pleura (1 of 5 pigs). It is important to note that this study was not designed to evaluate metastases, and most pigs did not have a complete necropsy, so the actual incidence of metastases is unknown. In addition, it is unknown whether these are true metastases. The peritoneal tumors could be due to leakage into the peritoneum during liver inoculation, and the lung tumor could be due to inoculation into the hepatic vein.

Overall features were similar to those of poorly differentiated to undifferentiated carcinomas, with or without multinucleated giant cells, of the human pancreatobiliary tract (32,33).

Embolization

After transarterial embolization, noncontrast CT showed retained contrast medium in the tumors (**Fig 4a, b**). Follow-up contrast-enhanced CT scan showed decreased size and enhancement of tumors after embolization (**Fig 4c**). Untreated tumors grew by 0.3 cm between 1 and 2 weeks after inoculation (**Fig 5**). In the same time interval, tumors shrank by 0.2 cm after embolization using 40–120 μm Embosphere microspheres ($P = .03$), and they shrank by 0.3 cm after embolization using 100–300 μm Embosphere microspheres ($P = .07$).

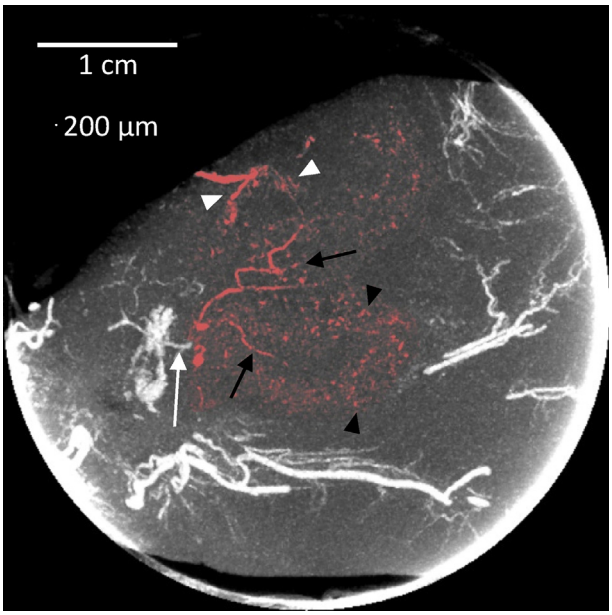

Figure 2. Micro-CT of a liver tumor in the Oncopig after intra-arterial injection of radiopaque silicone (maximum intensity projection image, 10-mm-thick slab, with tumor vessels colored red). The image shows a 0.3-mm tumor feeding artery (white arrow) (3 other feeding vessels not shown), branching intratumoral arteries (black arrows), disorganized intratumoral vessels (white arrowheads), and tiny vascular lakes (black arrowheads). The intratumoral vessels measure up to 0.5 mm, and the vascular lakes measure up to 1 mm. Scan resolution is 85 µm, and a 1-cm bar and 200-µm circle are shown for scale.

Complications

The complication rate was 25% (2 of 8 pigs). One pig treated with 40–120 µm Embosphere microspheres developed post-embolization syndrome (vomiting) requiring euthanasia. One pig treated with 100–300 µm Embosphere microspheres died during sedation for final imaging and was found to have a large right pleural effusion, liver infarct, and progressive extrahepatic metastases (peritoneum, lung). Histopathology showed Embosphere microspheres in both the hepatic artery and the portal vein, which could explain the liver infarct.

DISCUSSION

This study presents a promising new pig liver tumor model, with fast and reproducible site-specific tumor induction. The liver tumors are hypovascular, with a hypervascular rim, macrovascular invasion, and metastases in some cases. Histopathology showed poorly differentiated to undifferentiated carcinomas with a major inflammatory component. Oncopig liver tumor blood supply is similar to human liver tumors, and the tumors respond to transarterial embolization. The tumors can invade the portal vein or hepatic vein, similar to HCC. Comparison with other animal models is summarized in **Table E2** (available online on the article's Supplemental Material page at *www.jvir.org*) (16–22,25,26,34,35).

Oncopig liver tumor vascularity was characterized on both perfusion CT and micro-CT. Perfusion parameters in

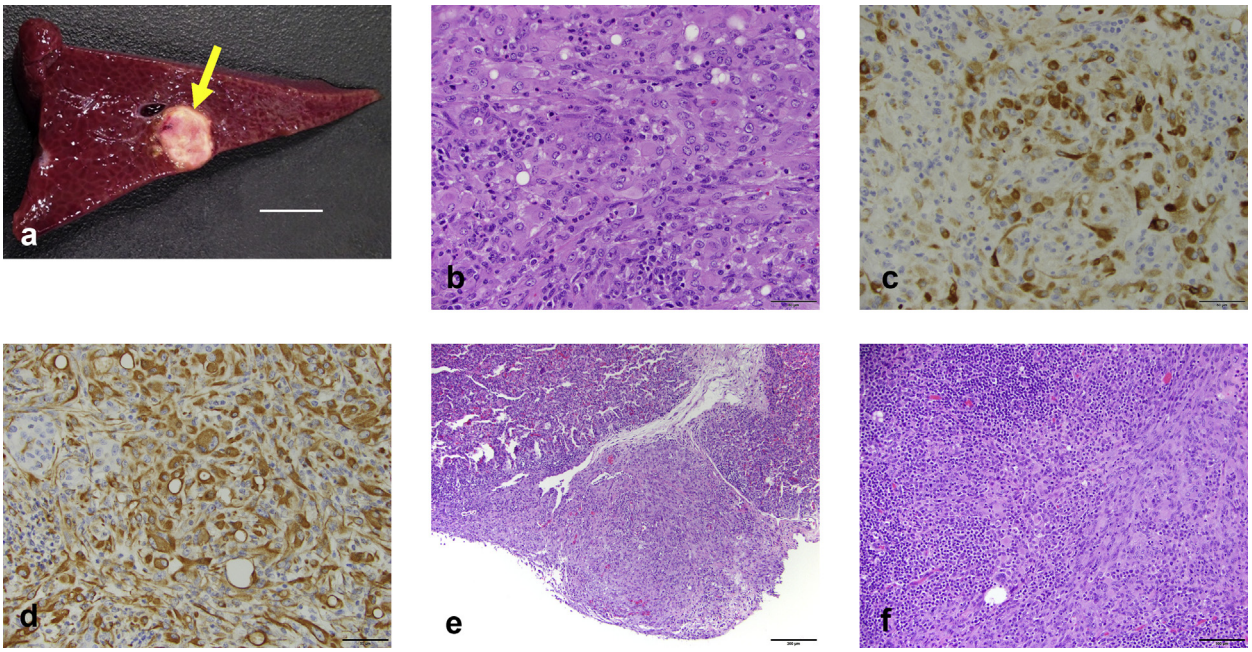

Figure 3. Pathology of Oncopig tumors. **(a)** Gross pathology shows a pale tan, well-circumscribed soft tissue nodule (arrow) in the liver (scale bar = 1 cm). **(b)** Hematoxylin and eosin–stained section shows that the tumor is composed of solid islands of atypical cells with eosinophilic cytoplasm and large nuclei (scale bar = 50 µm). **(c)** Cytokeratin AE1/AE3 expression (brown) in atypical cells confirms epithelioid differentiation (scale bar = 50 µm). **(d)** Vimentin immunopositivity (brown) confirms mesenchymal differentiation (scale bar = 50 µm). **(e)** Lung metastasis (scale bar = 200 µm). **(f)** Lymph node metastasis (scale bar = 100 µm). Additional immunohistochemistry is shown in **Figure E4**.

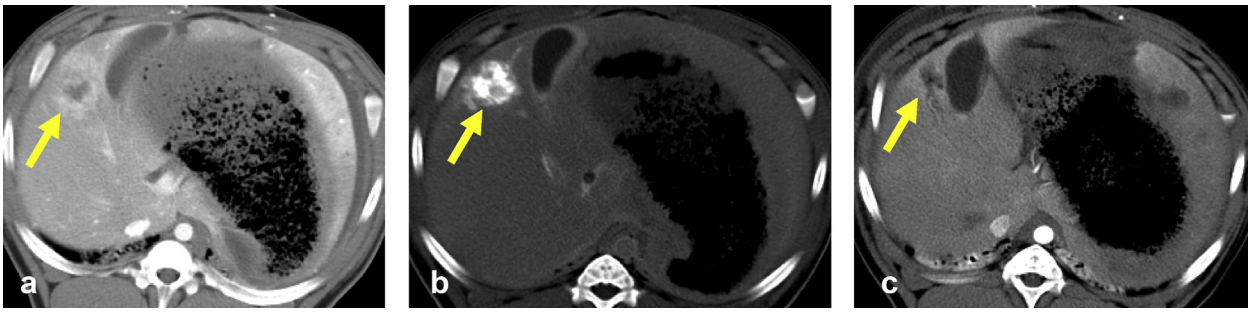

Figure 4. Transarterial embolization. **(a)** Contrast-enhanced CT shows an Oncopig liver tumor before treatment. **(b)** After transarterial embolization of the liver tumor using 40–120 μm Embosphere microspheres, noncontrast CT obtained immediately after the procedure shows retained contrast medium in the tumor. **(c)** Follow-up contrast-enhanced scan obtained 1 week later shows decreased size and enhancement of the liver tumor.

human liver tumors predict response to radioembolization of colorectal liver metastases (31) and survival after embolization of HCC (30). This study shows that Oncopig liver tumors have hepatic artery and portal vein perfusion characteristics that overlap with both human colorectal liver metastases and HCC.

Micro-CT of Oncopig liver tumors shows how the tumors recruit blood supply and develop tumor neovascularity. The tumors contain vascular lakes, which are also seen in human HCC (36), where they predict response to chemoembolization. Characterization of microscopic tumor vasculature down to the arteriole level (at the size of embolization particles) could provide insights into tumor angiogenesis and outcomes after therapy. Necropsy and micro-CT can provide detailed feedback on the causes of treatment failure and complications, which are not easily obtained in humans. For example, in an Oncopig with liver infarcts after embolization, necropsy showed embolic particles in both the hepatic artery and the portal vein, suggesting an angiographically occult arterioportal fistula as the cause of the infarct.

A major inflammatory component was seen in all of the Oncopig liver tumors. Undifferentiated carcinomas in humans can also contain an inflammatory infiltrate (32,33). Subcutaneous and intramuscular tumors in the Oncopig also contain a major inflammatory component, which is due to an antitumor T-cell response (37). Future experiments should address whether these inflammatory pig tumors could serve as a good model for the antitumor immune response in humans.

The cells of origin of these neoplasms could not be determined. Expression of cytokeratins and vimentin indicates epithelial and mesenchymal differentiation, respectively, and coexpression of these markers, in association with tumor morphology observed on hematoxylin and eosin–stained sections, is most consistent with a primary undifferentiated carcinoma undergoing epithelial-to-mesenchymal transition. Alternatively, the heterogeneous appearance of the tumors could be due to transformation of $>$ 1 cell type. Major epithelial populations of the liver that can give rise to carcinomas are hepatocytes and biliary epithelial cells. Arginase, a

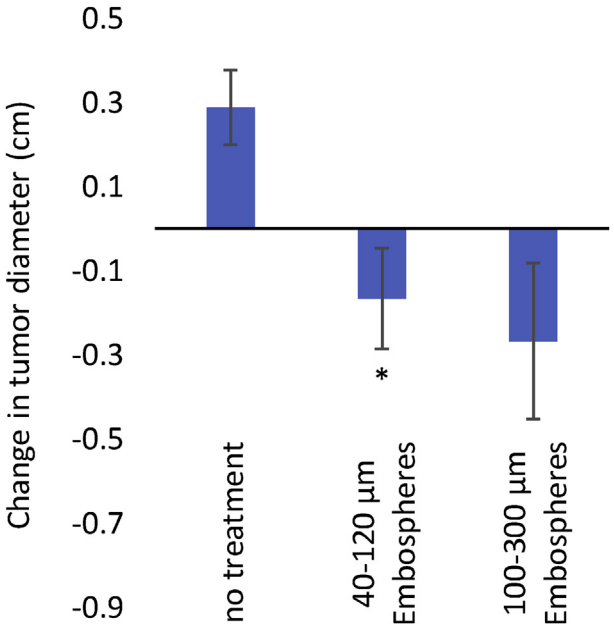

Figure 5. Change in liver tumor size 1 week after transarterial embolization compared with untreated tumors. After embolization using 40–120 μm Embosphere microspheres, tumor size decreased (P = .03) compared with untreated tumors. Other pairwise comparisons were not statistically significant. Error bars show standard error of the mean.

hepatocyte marker, was not expressed by tumor cells, but this lack of expression does not rule out a hepatocellular origin, as expression can be lost in undifferentiated tumors. There was no difference in histologic appearance of tumors generated using the cell line technique (which involved transforming purified hepatocytes) and the in situ technique (which involved transforming a core biopsy specimen of the liver, which contains both epithelial and mesenchymal cell types).

The Oncopig model has previously been used to generate subcutaneous and intramuscular tumors (28,38), but not liver tumors. Other pig liver tumor models are available (39), but they require $>$ 1 year for tumor development, which makes it difficult to rapidly test and iterate new

therapies. The simplified single-step tumor inoculation method reported here (in situ method) is technically simpler to implement than the cell line method, which requires liver resection and cell culture, and the rabbit VX2 model, which requires growing tumors subcutaneously before transferring them to the liver. The in situ tumor inoculation method can be performed by any interventional radiologist with access to an animal laboratory.

The Oncopig liver tumor model can be used to develop new image-guided therapies, such as tumor-targeting intra-arterial drug carriers (40), and intra-arterial local immunotherapy (41). One limitation of the Oncopig model is that it is more expensive than small animal models (but possibly easier to translate to human trials). Another limitation is that the inflammatory, poorly differentiated, rapidly growing tumors might not be a good model for well-differentiated or slowly growing tumors. However, the similarity in perfusion to human liver tumors and the response to bland embolization suggest that it will be a good model for arterially directed therapies and local drug delivery. The robust antitumor immune response could be helpful for developing new immunotherapy techniques.

In conclusion, liver tumors can be induced in a transgenic pig and can be successfully treated using bland embolization. The Oncopig liver tumor model is a potential alternative to the rabbit VX2 model, especially in cases where animal size or physiology are important.

ACKNOWLEDGMENTS

This work was supported by the Office of the Assistant Secretary of Defense for Health Affairs through the Peer Reviewed Cancer Research Program under Award No. W81XWH-16-1-0338. Opinions, interpretations, conclusions, and recommendations are those of the authors and are not necessarily endorsed by the Department of Defense. Some pigs were supplied by the National Swine Resource and Research Center, which was supported by National Institutes of Health Grant U42 OD011140. Our animal facility was supported in part by GE Healthcare, and core facilities were funded in part through an National Institutes of Health/National Cancer Institute Cancer Center Support Grant (P30 CA008748).

Govind Srimathveeravalli provided valuable advice. Megin Reilly, Lee-Ronn Paluch, Jacqueline Candelier, Brian Hanna, Stephanie Harris-Ash, Alvin Lopez, and Brian Cuevas helped with animal experiments. Liqun Cai helped with cell culture experiments. Afsar Barlas, Maria Jiao, and Mesruh Turkekul performed immunohistochemistry. Regina Schwind helped coordinate experiments.

REFERENCES

1. Duran-Struuck R, Huang CA, Matar AJ. Cellular therapies for the treatment of hematological malignancies; swine are an ideal preclinical model. Front Oncol 2019; 9:418.
2. Poursaid A, Jensen MM, Nourbakhsh I, et al. Silk-elastinlike protein polymer liquid chemoembolic for localized release of doxorubicin and sorafenib. Mol Pharm 2016; 13:2736–2748.
3. Sudheendra D, Leger R, Groppo ER, et al. Comparison of three different needles for percutaneous injections. Cardiovasc Intervent Radiol 2007; 30:151–152.
4. Titano JJ, Fischman AM, Cherian A, et al. End-hole versus microvalve infusion catheters in patients undergoing drug-eluting microspheres-TACE for solitary hepatocellular carcinoma tumors: a retrospective analysis. Cardiovasc Intervent Radiol 2019; 42:560–568.
5. Mathios D, Kim JE, Mangraviti A, et al. Anti-PD-1 antitumor immunity is enhanced by local and abrogated by systemic chemotherapy in GBM. Sci Transl Med 2016; 8(370ra180).
6. Kim GM, Kim MD, Kim do Y, et al. Transarterial chemoembolization using sorafenib in a rabbit VX2 liver tumor model: pharmacokinetics and antitumor effect. J Vasc Interv Radiol 2016; 27:1086–1092.
7. Yarmohammadi H, Wilkins LR, Erinjeri JP, et al. Efficiency of combined blocking of aerobic and glycolytic metabolism pathways in treatment of N1-S1 hepatocellular carcinoma in a rat model. J Cancer Res Ther 2017; 13:533–537.
8. Lee IJ, Lee M, Kim SJ, Kim YK, Won JY, Chung JW. Chemoembolization with vascular disrupting agent CKD-516 dissolved in ethiodized oil in combination with doxorubicin: a VX2 tumor model study. J Vasc Interv Radiol 2018; 29:1078–1084.
9. Duran R, Namur J, Pascale F, et al. Vandetanib-eluting radiopaque beads: pharmacokinetics, safety, and efficacy in a rabbit model of liver cancer. Radiology 2019; 293:695–703.
10. Zhang X, Dai F, Chen J, et al. Antitumor effect of curcumin liposome after transcatheter arterial embolization in VX2 rabbits. Cancer Biol Ther 2019; 20:642–652.
11. Liu Y, Zhang Y, Bautista D, et al. Trans-arterial p53-gene-embolization with gelatin sponge microparticles for hepatocellular carcinoma with BCLC stage B: single-center experience. Cell Biochem Biophys 2015; 71:99–104.
12. Cressman ENK, Guo C, Karbasian N. Image-guided chemistry altering biology: an in vivo study of thermoembolization. PLoS One 2018; 13: e0200471.
13. Attaluri A, Seshadri M, Mirpour S, et al. Image-guided thermal therapy with a dual-contrast magnetic nanoparticle formulation: a feasibility study. Int J Hyperthermia 2016; 32:543–557.
14. Xu J, Cheng X, Tan L, et al. Microwave responsive nanoplatform via P-selectin mediated drug delivery for treatment of hepatocellular carcinoma with distant metastasis. Nano Lett 2019; 19:2914–2927.
15. White SB, Kim DH, Guo Y, et al. Biofunctionalized hybrid magnetic gold nanoparticles as catalysts for photothermal ablation of colorectal liver metastases. Radiology 2017; 285:809–819.
16. Asgharpour A, Cazanave SC, Pacana T, et al. A diet-induced animal model of non-alcoholic fatty liver disease and hepatocellular cancer. J Hepatol 2016; 65:579–588.
17. Gade TP, Hunt SJ, Harrison N, et al. Segmental transarterial embolization in a translational rat model of hepatocellular carcinoma. J Vasc Interv Radiol 2015; 26:1229–1237.
18. Mak IW, Evaniew N, Ghert M. Lost in translation: animal models and clinical trials in cancer treatment. Am J Transl Res 2014; 6:114–118.
19. West GB, Brown JH, Enquist BJ. A general model for the origin of allometric scaling laws in biology. Science 1997; 276:122–126.
20. Schmidt-Nielsen K. Scaling: Why Is Animal Size So Important? New York: Cambridge University Press; 1984.
21. Nair AB, Jacob S. A simple practice guide for dose conversion between animals and human. J Basic Clin Pharm 2016; 7:27–31.
22. Sharma V, McNeill JH. To scale or not to scale: the principles of dose extrapolation. Br J Pharmacol 2009; 157:907–921.
23. Schook LB, Collares TB, Hu W, et al. A genetic porcine model of cancer. PloS One 2015; 10:e0128864.
24. Boas FE, Nurili F, Bendet A, et al. Induction and characterization of pancreatic cancer in a transgenic pig model. PloS One 2020; 15: e0239391.
25. Overgaard NH, Frosig TM, Welner S, et al. Establishing the pig as a large animal model for vaccine development against human cancer. Front Genet 2015; 6:286.
26. Dawson HD, Smith AD, Chen C, Urban JF Jr. An in-depth comparison of the porcine, murine and human inflammasomes; lessons from the porcine genome and transcriptome. Vet Microbiol 2017; 202:2–15.
27. National Research Council (US) Committee for the Update of the Guide for the Care and Use of Laboratory Animals. *Guide for the care and use of laboratory animals*. 8th ed. Washington, DC: National Academies Press; 2011.
28. Schachtschneider KM, Schwind RM, Darfour-Oduro KA, et al. A validated, transitional and translational porcine model of hepatocellular carcinoma. Oncotarget 2017; 8:63620–63634.

29. Gaba RC, Elkhadragy L, Boas FE, et al. Development and comprehensive characterization of porcine hepatocellular carcinoma for translational liver cancer investigation. Oncotarget 2020; 11:2686–2701.
30. Borgheresi A, Gonzalez-Aguirre A, Brown KT, et al. Does enhancement or perfusion on preprocedure CT predict outcomes after embolization of hepatocellular carcinoma? Acad Radiol 2018; 25:1588–1594.
31. Boas FE, Brody LA, Erinjeri JP, et al. Quantitative measurements of enhancement on preprocedure triphasic CT can predict response of colorectal liver metastases to radioembolization. AJR Am J Roentgenol 2016; 207:671–675.
32. Muraki T, Reid MD, Basturk O, et al. Undifferentiated carcinoma with osteoclastic giant cells of the pancreas: clinicopathologic analysis of 38 cases highlights a more protracted clinical course than currently appreciated. Am J Surg Pathol 2016; 40:1203–1216.
33. Reid MD, Basturk O, Thirabanjasak D, et al. Tumor-infiltrating neutrophils in pancreatic neoplasia. Mod Pathol 2011; 24:1612–1619.
34. Dawson HD, Loveland JE, Pascal G, et al. Structural and functional annotation of the porcine immunome. BMC Genomics 2013; 14:332.
35. Seok J, Warren HS, Cuenca AG, et al. Genomic responses in mouse models poorly mimic human inflammatory diseases. Proc Natl Acad Sci U S A 2013; 110:3507–3512.
36. Cavalcante RN, Nasser F, Motta-Leal-Filho JM, et al. Occurrence of vascular lake phenomenon as a predictor of improved tumor response in HCC patients that underwent DEB-TACE. Cardiovasc Intervent Radiol 2017; 40:1044–1051.
37. Overgaard NH, Principe DR, Schachtschneider KM, et al. Genetically induced tumors in the Oncopig model invoke an antitumor immune response dominated by cytotoxic CD8beta(+) T cells and differentiated gammadelta T cells alongside a regulatory response mediated by FOXP3(+) T cells and immunoregulatory molecules. Front Immunol 2018; 9:1301.
38. Schachtschneider KM, Liu Y, Makelainen S, et al. Oncopig soft-tissue sarcomas recapitulate key transcriptional features of human sarcomas. Sci Rep 2017; 7:2624.
39. Li X, Zhou X, Guan Y, Wang YX, Scutt D, Gong QY. N-nitrosodiethylamine-induced pig liver hepatocellular carcinoma model: radiological and histopathological studies. Cardiovasc Intervent Radiol 2006; 29:420–428.
40. Nurili F, Yarmohammadi H, Bendet A, et al. Improved intra-arterial tumor targeting using an omniphobic oil in a pig model. J Vasc Interv Radiol 2019; 30:S204.
41. Boas FE, Nurili F, Erinjeri JP, Schook LB, Solomon SB, Yarmohammadi H. Local immunotherapy: intra-arterial liver tumor vaccination in a pig model of metastatic pancreatic cancer. J Vasc Interv Radiol 2019; 30:S98–S99.

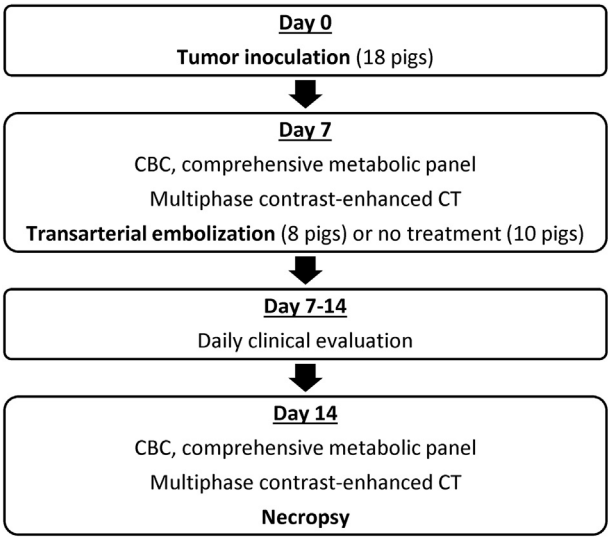

Figure E1. Study design. CBC = complete blood count.

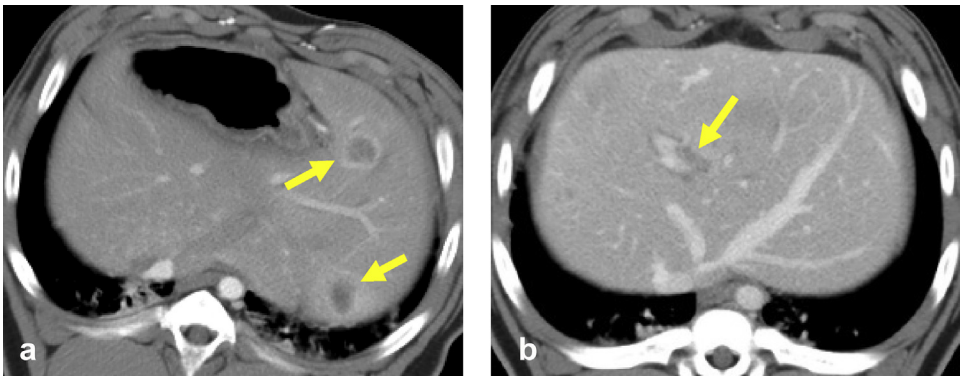

Figure E2. Contrast-enhanced CT shows that some Oncopig liver tumors (arrows) have hypervascular rims **(a)** or invade the portal vein **(b)**.

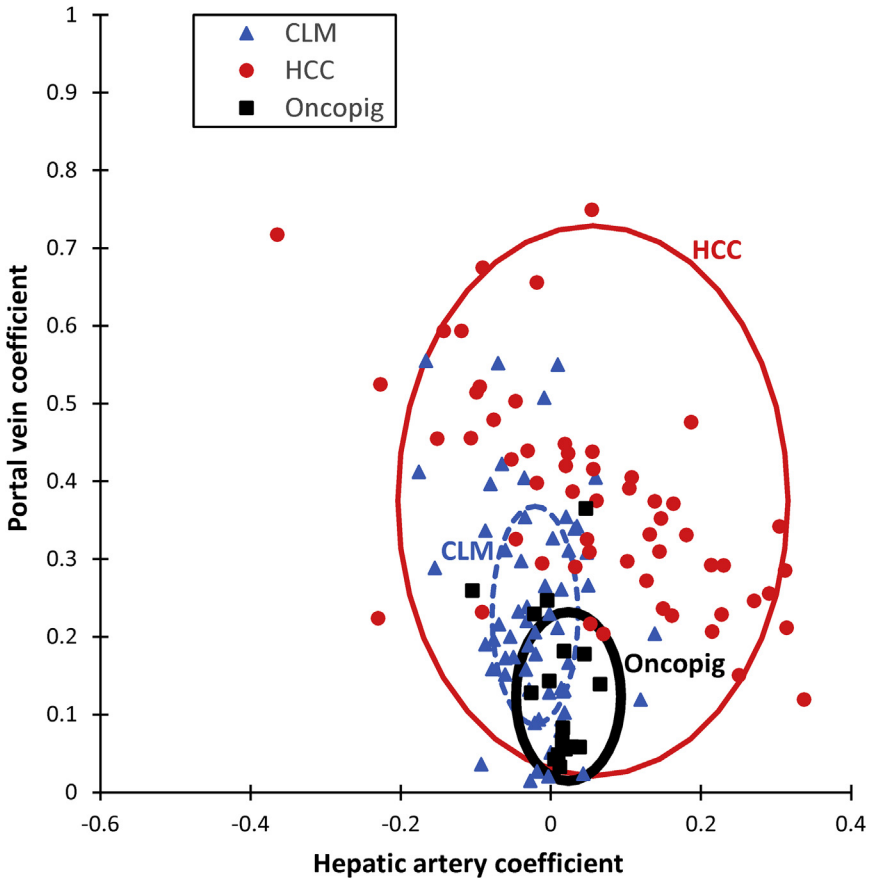

Figure E3. Hepatic artery and portal vein perfusion of Oncopig liver tumors compared with previously published perfusion measurements on human hepatocellular carcinoma (*HCC*) (30) and human colorectal liver metastases (*CLM*) (31). The hepatic artery coefficient is an estimate of the hepatic artery blood supply to a liver tumor, and the portal vein coefficient is an estimate of the portal vein blood supply to the tumor. Each point represents a single tumor. The ellipses show the average ± SD for each group.

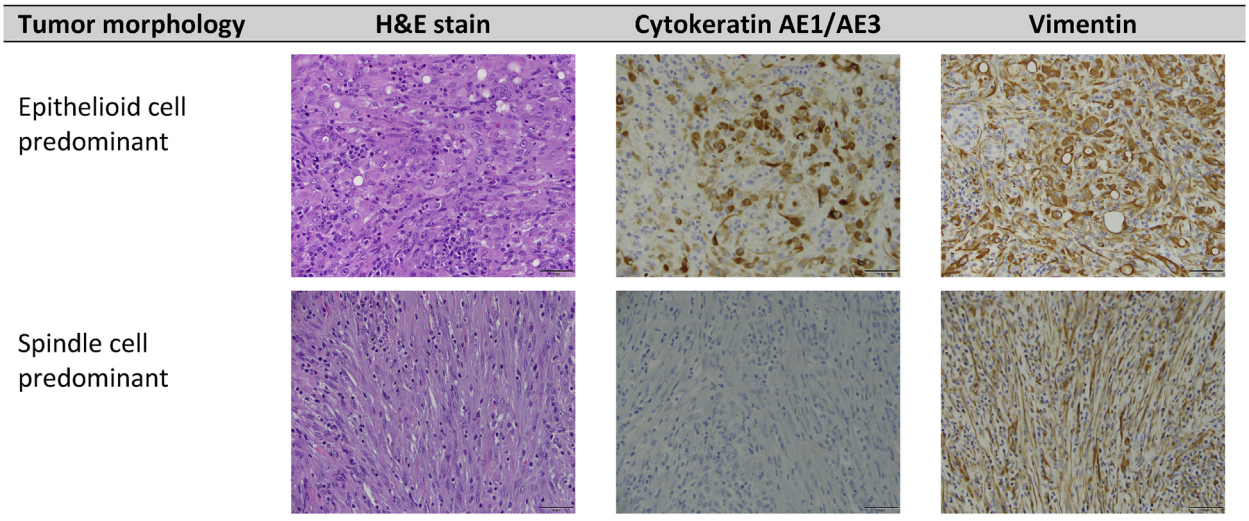

Figure E4. Immunohistochemistry of Oncopig liver tumors shows that atypical epithelioid cells were immunopositive (brown) for both cytokeratin AE1/AE3 and vimentin. Spindle cells were immunopositive (brown) for vimentin, but immunonegative for cytokeratin AE1/AE3. Scale bars = 50 μm. H&E = hematoxylin and eosin.

Table E1. Immunohistochemistry Technique

Marker	Staining Platform	Epitope Retrieval	Primary Antibody	Primary Antibody Concentration	Secondary Antibody and Detection System
Cytokeratin AE1/AE3	Ventana XT*	Tris EDTA–based CC1 retrieval†, pH 8	760-2135†	Prediluted, 1:5	MKB-2225‡, Ventana DAB Map*
Vimentin	BOND RX§	Heat-induced, pH 9.0	5741‖	1:250	DS9800§
Iba1	BOND RX	Heat-induced, pH 9.0	ab5076¶	1:500	BA-5000‡, DS9800§
Arginase	Manual	Heat-induced, pH 6.0	ab91279¶	1:1,000	BA-1000, PK-6100‡
CD31	Manual	Tri EDTA	ab28364¶	1:100	BA-1000

*Roche Diagnostics Corp, Indianapolis, Indiana.
†Ventana Medical Systems, Oro Valley, Arizona.
‡Vector Laboratories, Inc, Burlingame, California.
§Leica Biosystems, Inc, Buffalo Grove, Illinois.
‖Cell Signaling Technology, Danvers, Massachusetts.
¶Abcam, Cambridge, Massachusetts.

Table E2. Animal Models of Primary or Secondary Liver Cancer

	Oncopig	Rabbit VX2	Rat/Mouse
Histology	Carcinoma, with inflammatory infiltrate	Squamous cell carcinoma, with necrosis before treatment	HCC (16,17)
Site-specific tumor induction	Yes	Yes	No
Devices/catheters	Same as humans	Requires smaller devices/ catheters	Requires smaller devices/ catheters
Blood supply to liver	Mostly portal vein (similar to humans)	Mostly portal vein (similar to humans)	More dependent on hepatic artery flow; hepatic artery is same size as portal vein; high rate of death after lobar TAE (17)
Drug dosing	Similar to human weight-based dosing (21,22)	Usually higher mg/kg dosing than humans; different pharmacokinetics	Usually higher mg/kg dosing than humans; different pharmacokinetics
Metabolic rate or oxygen use (per kg)	Similar to humans	Higher for smaller animals	Higher for smaller animals (19,20)
Immune response	Strong antitumor immune response; pig immunome is similar to humans (25,26,34)	Unknown	Immune response differs from humans (35)
Translatability	Unknown	Unknown	High failure rate when therapies are translated to humans (18)

HCC = hepatocellular carcinoma; TAE = transarterial embolization.